






## Viscoelastic behavior of chemically fueled supramolecular hydrogels under load and influence of reaction side products

Martin Kretschmer <sup>1,2</sup>, Benjamin Winkeljann <sup>1,2</sup>✉, Brigitte A. K. Kriebisch <sup>3,4</sup>, Job Boekhoven <sup>3,4</sup> & Oliver Lieleg <sup>1,2</sup>✉

About ten years ago, chemically fueled systems have emerged as a new class of synthetic materials with tunable properties. Yet, applications of these materials are still scarce. In part, this is due to an incomplete characterization of the viscoelastic properties of those materials, which has - so far - mostly been limited to assessing their linear response under shear load. Here, we fill some of these gaps by comparing the viscoelastic behavior of two different, carbodiimide fueled Fmoc-peptide systems. We find that both, the linear and non-linear response of the hydrogels formed by those Fmoc-peptides depends on the amount of fuel driving the self-assembly process - but hardly on the direction of force application. In addition, we identify the concentration of accumulated waste products as a novel, so far neglected parameter that crucially affects the behavior of such chemically fueled hydrogels. With the mechanistic insights gained here, it should be possible to engineer a new generation of dynamic hydrogels with finely tunable material properties that can be tailored precisely for such applications, where they are challenged by mechanical forces.

<sup>1</sup>Department of Mechanical Engineering and Munich School of Bioengineering, Technical University of Munich, Boltzmannstraße 15, 85748 Garching, Germany. <sup>2</sup>Center for Protein Assemblies (CPA), Ernst-Otto-Fischer Straße 8, 85748 Garching, Germany. <sup>3</sup>Department of Chemistry, Technical University of Munich, Lichtenbergstrasse 4, 85748 Garching, Germany. <sup>4</sup>Institute for Advanced Study, Technical University of Munich, Lichtenbergstrasse 2a, 85748 Garching, Germany. ✉email: [benjamin.winkeljann@tum.de](mailto:benjamin.winkeljann@tum.de); [oliver.lieleg@tum.de](mailto:oliver.lieleg@tum.de)

Inspired by the dynamic assembly and disassembly of biomolecules at the expense of chemical energy<sup>1,2</sup>, intensive research has been conducted to understand the molecular mechanisms driving this self-assembly process to develop artificial analogs<sup>3–10</sup>. Both, biological and man-made, chemically fueled dynamic materials dramatically differ from in-equilibrium materials as they exist outside of thermodynamic equilibrium; in other words, a driving force is necessary to obtain and maintain these materials in their non-equilibrium state<sup>11,12</sup>. One strategy to achieve such a dynamic behavior is by using fuel-driven reaction cycles<sup>13–21</sup>. Here, the energy required to keep the material out of equilibrium is generated by the irreversible conversion of a “fuel” molecule. In nature, a prominent example for such a fuel-based assembly process can be found in the cytoskeleton:<sup>22</sup> here, the building blocks of the actin cortex (i.e., G-actin subunits) assemble into filaments (F-actin) by consuming energy provided by the hydrolysis of ATP<sup>23,24</sup>. Pioneering work in synthetically recreating this reaction was done in the 2010s by van Esch and coworkers, who presented a chemical reaction cycle that catalyzes the hydrolysis of methylating agents<sup>25</sup>. Since then, various other strategies and reaction cycles have been introduced<sup>18</sup>. Whereas the main idea remains the same in all those examples, many different, fascinating systems have been presented including pulsating micelles<sup>26</sup>, self-assembling metal-organic framework systems<sup>27</sup>, or loadable, DNA-based actuators<sup>28</sup>.

In 2017, Tena-Solsona et al. introduced chemically fueled materials based on fluorenylmethoxycarbonyl (Fmoc)-protected peptides<sup>29</sup>. Here, self-assembly is driven by the hydration of a carbodiimide fuel. In such Fmoc-based peptide systems, the properties of the self-assembled materials are broadly tunable, and this is achieved by a tailored variation of the conjugated amino acid sequence<sup>29</sup>. In detail, supramolecular structures with tunable shape, size, and lifetime could be created. Although the reaction kinetics governing the lifecycle of such assembled structures have been investigated extensively, one detail remains partially neglected: the role of waste products. Compared to biological systems, where the concentrations of the contributing molecular components are strictly regulated by the cellular machinery, such control is difficult to achieve in closed, artificial systems; here, waste products accumulate over the lifetime of the material. It was speculated previously that the reaction waste products might interact with the supramolecular structures and disturb their assembly process<sup>30</sup>. To avoid such interference by waste accumulation effects, Sorrenti et al. created dynamic self-assemblies in a membrane reactor which allowed waste molecules to leave the microcompartment<sup>31</sup>.

The micro- and mesoscopic properties of such supramolecular assemblies, especially fiber-forming peptides, also directly impact macroscopic material characteristics. Specifically, a dynamic transition from a solution into a gel (and back) was observed, and those transitions were shown to follow the kinetics of the molecular assembly process<sup>29,32</sup>. Depending on the detailed structures generated during the self-assembly procedure, the lifetime of such macroscopic gels can be broadly tunable. Yet, so far, experimental studies investigating the mechanical properties of such out-of-equilibrium materials were limited to the linear response regime<sup>32–34</sup>. The nonlinear behavior of these chemically fueled materials has been underexplored. Partially this might be caused by the fact that both the exact point where Hooke’s law does not hold true anymore and the type of nonlinear material response setting in beyond this point cannot easily be predicted; instead, both items require separate investigations using the specialized methodology. Such nonlinear material properties are, however, relevant when a material is exposed to a large mechanical load—be it shear or compression forces. Depending on the application area such (or similar) self-assembling, dynamic materials might

be further developed; in the future, such material behavior under load can be highly important.

Here, we investigate the macroscopic material properties of hydrogels formed by two different self-assembling (Fmoc)-protected peptides derivatives. We first characterize both, the linear and nonlinear viscoelastic properties of these two systems with respect to initial fuel concentration and time. Then, we assess the failure behavior of the hydrogel materials when exposed to different levels of mechanical stress. We demonstrate how the waste products generated by the fuel conversion affects the mechanical properties of the hydrogels—both, when added to the system prior to gel formation and when accumulating within the system over time. By comparing results obtained with the full waste product to data obtained with waste-mimetics, we identify hydrophobic and (to a lower extent) electrostatic interactions between the Fmoc-based peptides and the waste molecules to be the critical forces that challenge the assembly process. Furthermore, our results suggest that the molecular design of the peptide sequence plays a critical role for how waste accumulation influences the dynamic self-assembly/disassembly process.

## Results and discussion

**Peptide design and dynamic assembly process.** Dynamic self-assembling hydrogels based on Fmoc-protected peptides (Fmoc-aa) derivatives have been introduced previously<sup>29</sup>. When solubilized in a suitable aqueous buffer system, the anionic peptides repel each other through electrostatic forces established by the dicarboxylate groups. The peptides are designed to react with a carbodiimide-based fuel in an activation reaction. Upon activation, the dicarboxylate-based precursor is converted into its corresponding cyclic anhydride at the expense of 1-ethyl-3-(3-dimethylaminopropyl)carbodiimid-hydrochlorid (EDC) which is converted in 1-[3-(dimethylamino)propyl]-3-ethylurea (EDU). In the aqueous environment, the activated anhydride state is not stable and will spontaneously hydrolyze to yield its precursor state (Fig. 1a). Thus, when fuel is added to the precursor, a population of transiently activated anhydride product is obtained. In this anhydride state, the electrostatic repulsion between the molecules is eliminated, which results in their assembly. However, due to the transient nature of the anhydride, a dynamic assembly is created which is regulated through the kinetics of activation and deactivation. When a finite amount of fuel is added, assemblies emerge with a finite lifetime. The range of assemblies that can be obtained by using EDC as fuel includes colloids<sup>35</sup>, vesicles<sup>36</sup>, oil-based<sup>37,38</sup> and coacervate-based<sup>39,40</sup> droplets, and hydrogel-forming fibers<sup>32</sup>.

In the peptide design, the repulsive and attractive forces must be balanced such that the precursor remains in solution but the product assembles. Two possible peptide sequences that allow for such controlled self-assembly of Fmoc-peptide-conjugates into supramolecular structures are Fmoc-alanine–valine–aspartic acid (Fmoc-AVD) and Fmoc-alanine–alanine–aspartic acid (Fmoc-AAD) (Fig. 1b). Here, the substitution of valine with alanine slightly reduces the hydrophobic character of the tripeptide. As a consequence of this small modification, a larger proportion of the Fmoc-constructs can be expected to switch into the disassembled state thus rendering supramolecular aggregates less pronounced<sup>41</sup>. Furthermore, as demonstrated previously using confocal microscopy and cryo-TEM imaging, this modification also alters the morphology of the assembled structures from wide, flat fibers (obtained for Fmoc-AVD) into thinner, more twisted helical structures (observed for Fmoc-AAD)<sup>41</sup>.

**Rheological behavior of dynamic peptide-based hydrogels.** When we investigate the time-dependent viscoelastic moduli of

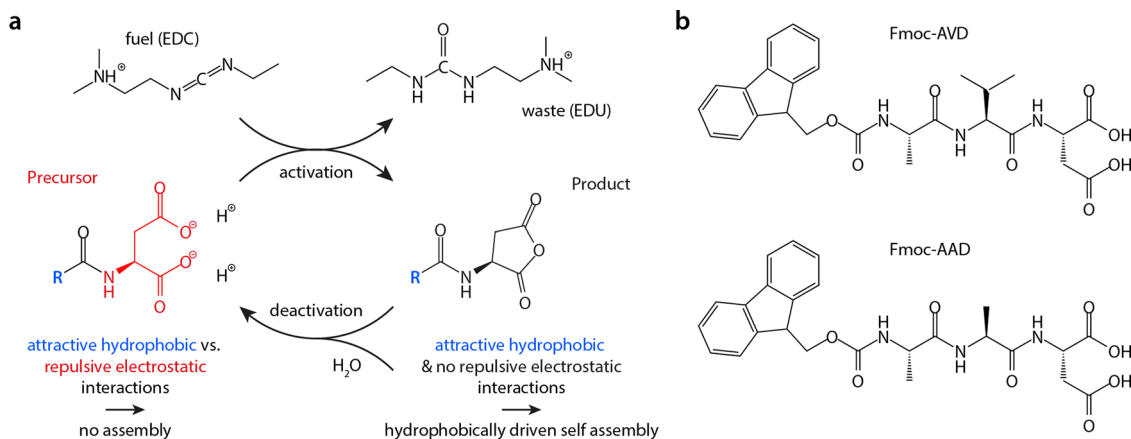


**Fig. 1 Schematic illustration of the reaction cycle and peptide precursors used in this study.** **a** In the activation reaction, aspartic acid derivatives of the precursor peptide react in the presence of a suitable fuel (here: EDC) and are converted into their corresponding anhydride product; at the same time, a waste product (here: EDU) is generated. In the deactivation reaction, the aspartic acid anhydride derivative is hydrolyzed again. Through the correct design of the Fmoc-peptides, attractive and repulsive forces can be balanced such that a hydrophobically driven self-assembly process is enabled—but only in the product state. Hydrophobic sidechains are depicted in blue and anionic ones in red. **b** Structural formula of the two synthetic Fmoc-peptides used here.

the Fmoc-AVD hydrogels, we observe a behavior consistent with the underlying reaction cycle driving the dynamic self-assembly of the system: When the Fmoc-AVD samples are premixed with the “fuel”, the system is already in a hydrogel state when the rheological characterization starts, i.e., the material is dominated by elastic properties as represented by the storage modulus  $G'$ . Then, we observe a quick increase in both viscoelastic moduli, which reach their respective maxima within the first 2 min of the measurement. Afterward, both viscoelastic moduli slowly decrease over time and reach plateaus after ~15–20 min (Fig. 2a). Further changes in the viscoelastic properties of this system are not observable—even when the moduli are tracked for up to 120 min (Supplementary Results Section 1.1 and Supplementary Fig. 1). Macroscopically, the formation of supramolecular structures can be visualized by a transition from clear to turbid samples. In addition, confocal images give insight into the size and shape of the supramolecular clusters formed in the hydrogels (Fig. 2). Over time, the turbidity of samples created with low (100 mM) or medium (250 mM) EDC concentrations slightly decreases; however, inverted tube tests confirm the ongoing presence of an elastically dominated material (Supplementary Results Section 1.1 and Supplementary Fig. 2).

In previous work, it was shown that the time point, at which such a dynamic peptide hydrogel system reaches its highest elasticity, corresponds to the moment when the maximal anhydride concentration is present in the system<sup>29</sup>. The subsequent hydrolysis of this anhydride is responsible for a slow disassembly of the gel, which causes both viscoelastic moduli to decline. Yet, a certain amount of the Fmoc-AVD molecules remains trapped in self-assembled fibers even though they have returned into their initial, self-repelling precursor state. Thus, we hypothesize that such kinetically trapped fibers are responsible for the remaining elastic-dominated properties of the system, which persist even though all the fuel can be expected to be consumed.

Consistent with previous results obtained with similar systems<sup>29</sup>, the amount of fuel that is initially present affects the viscoelastic properties of the assembled hydrogel in two ways: first, increasing the fuel concentration from 100 to 250 mM extends the lifetime of the gel, i.e., it increases the time span beyond which the elastic properties of the system start to decrease (Fig. 2a). Second, such an increase in the fuel concentration also boosts the maximal elasticity of the gel (Fig. 2b).

However, further increasing the fuel concentration to 1000 mM only slightly affects the properties of the assembled hydrogel by weakly increasing its lifetime (Fig. 2a) without significantly increasing the maximal gel stiffness. This finding indicates that, at those particular conditions, the conversion reaction from precursor to anhydride has probably reached its maximum yield<sup>29</sup>. So far, we have assessed the viscoelastic properties of the Fmoc-AVD system in the linear response regime, i.e., a small mechanical load where Hooke’s law holds. When we probe the nonlinear properties of the same set of samples by large amplitude oscillatory shear (LAOS) measurements (where we continuously increase the oscillatory strain applied to the samples while tracking the viscoelastic moduli; see Methods section “LAOS measurements” for details), we find that all three Fmoc-AVD hydrogel variants show linear material response up to strain levels of  $\sim\gamma = 1\text{--}2\%$  (Fig. 2c). At this critical point, where the nonlinear response regime of the hydrogels is left, strain weakening sets in. The corresponding maximal stress levels we determine around those critical points range from  $26 \pm 5$  Pa (determined for 100 mM fuel) to  $82 \pm 8$  Pa (determined for 1000 mM fuel) (Supplementary Results Section 1.1 and Supplementary Fig. 3a).

Next, we use a similar approach to assess the viscoelastic properties of a system generated from a slightly different Fmoc-variant conjugated to the tripeptide AAD. In contrast to the Fmoc-AVD system discussed above, the AAD peptide provides the respective Fmoc-conjugate with significantly slower reaction kinetics<sup>29</sup>. Consequently, upon gelation, this system reaches its maximal elasticity a bit later than Fmoc-AVD, i.e., ~4–5 min after the addition of fuel. Moreover, the absolute values of the moduli reached here are lower than for Fmoc-AVD. This can be rationalized by differences in the attractive forces acting in both Fmoc-systems: by replacing the amino acid valine with alanine, the hydrophobicity of the peptide core part is decreased. This replacement should slightly shift the delicate balance between hydrophobic attractive and electrostatic repulsive forces towards the attractive forces. In addition, as discussed above, this replacement also entails a structural change of the supramolecular motifs generated by the Fmoc-peptides. Together, we consider this structural change and the increase in hydrophobic attractive forces to be one reason for the increased mechanical stability of Fmoc-AVD gels compared to Fmoc-AAD gels.

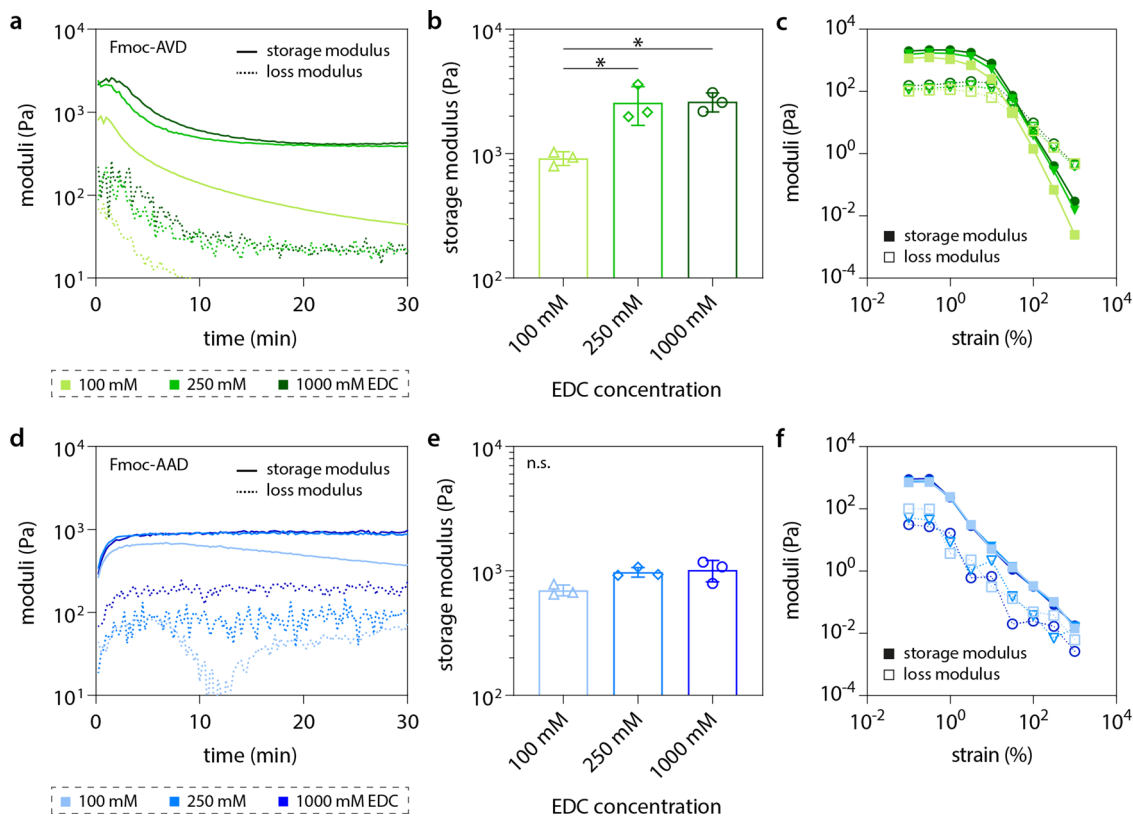


**Fig. 2** Viscoelastic properties of self-assembled hydrogels. The fuel concentration affects the time-dependent viscoelastic properties (a), the maximal storage modulus obtained during the reaction process (b), and the nonlinear mechanical properties (c) of self-assembled Fmoc-AVD hydrogels. The Fmoc-AAD system is influenced by different fuel concentrations in a similar manner (d–f); yet, the viscoelastic moduli stay in a plateau-like state once the gel is formed (d). Gelation curves (a, d) and LAOS measurements (c, f) show the mean of data obtained from  $n = 3$  independent samples. Bar plots in panels (b, e) represent the mean together with the standard deviation ( $n = 3$ , significance level  $p < 0.05$  as determined by ordinary one-way ANOVA and Tukey post hoc tests). Fmoc-AVD data is depicted in green and Fmoc-AAD data is in blue. Bright colors represent an EDC concentration of 100 mM, medium bright colors correspond to 250 mM, and dark colors to 1000 mM. Solid lines represent the storage modulus and dashed lines the loss modulus. Individual data points are depicted with triangles (100 mM EDC), rhombuses (250 mM EDC), and circles (1000 mM).

Moreover, once a stable gel is formed, we only observe a slight (if at all) decline in the viscoelastic properties over time (Fig. 2d). Also, here, the turbidity changes and the inverted tube tests and fluorescent images support our observations from the rheological investigations (Supplementary Results Section 1.1 and Supplementary Fig. 4). Based on previous studies, we expect this good stability of the hydrogel to originate from the fact that, when fuel is abundant, most of the supramolecular structures formed by Fmoc-AAD remain in their assembled state—even when the anhydride component is hydrolyzed into its precursor state<sup>41</sup>. Overall, the Fmoc-AAD system has properties that only weakly depend on the fuel concentration—both in the linear and nonlinear response regime (Fig. 2d–f). Similar to the Fmoc-AVD gels, also the Fmoc-AAD gel variants show strain weakening at strain levels above  $\sim \gamma = 1$ –2%, and the maximal stress levels, the samples withstand during this type of nonlinear shear rheology measurements, are all in the range of 2.5–3 Pa. (Supplementary Fig. 3b).

**Mechanical failure of hydrogel clogs in tubings.** Up to now, we have assessed the mechanical properties of the two Fmoc-systems when exposed to either low or high shear forces. We found that the shear resistance of Fmoc-AVD gels depends on the amount of fuel present in the system. In contrast, the viscoelastic properties of the Fmoc-AAD system exhibit only a weak dependence on the fuel concentration. In possible application scenarios, however, it is unlikely that the material will be exposed to shear forces

exclusively. Thus, in the next step, we aim at testing the same set of gels in an environment, where they can be exposed to normal load. For this purpose, we developed a fluidic system, which can be temporarily sealed using hydrogel clogs generated by the two Fmoc-based peptides. When injected into this fluidic system, the hydrogel clog can be exposed to an adjustable fluid pressure, which creates a defined normal load onto the hydrogel material (Fig. 3a, see Methods section “Transient clogging of fluidic systems” for details).

When determining the stress resistance of such dynamic hydrogel clogs, it is important to consider that two parameters affect the stability of the gels in the presence of mechanical load: the viscoelastic properties of the system as determined by the initial fuel concentration and the intrinsic lifetime of the created hydrogel system. For consistency, we test the maximal pressure resistance of each gel variant at the particular time point when the gel reaches its highest elasticity. When we seal the tubing with a Fmoc-AVD hydrogel clog containing 100 mM fuel and then continuously increase the applied fluid pressure, we observe clog failure at a “burst pressure” of  $\sim 20$  mbar. When increasing the fuel concentration to 250 mM, the stress resistance of the hydrogel clog is increased such that it withstands pressures up to  $\sim 30$  mbar (Fig. 3c). This result agrees well with the differences we observed in the maximum elastic moduli determined for those two Fmoc-AVD hydrogel variants in the linear response regime, i.e.,  $G'_{100} = 0.9 \pm 0.1$  kPa for 100 mM of fuel and  $G'_{250} = 2.6 \pm 0.9$  kPa for 250 mM of fuel (Fig. 2b). Interestingly,



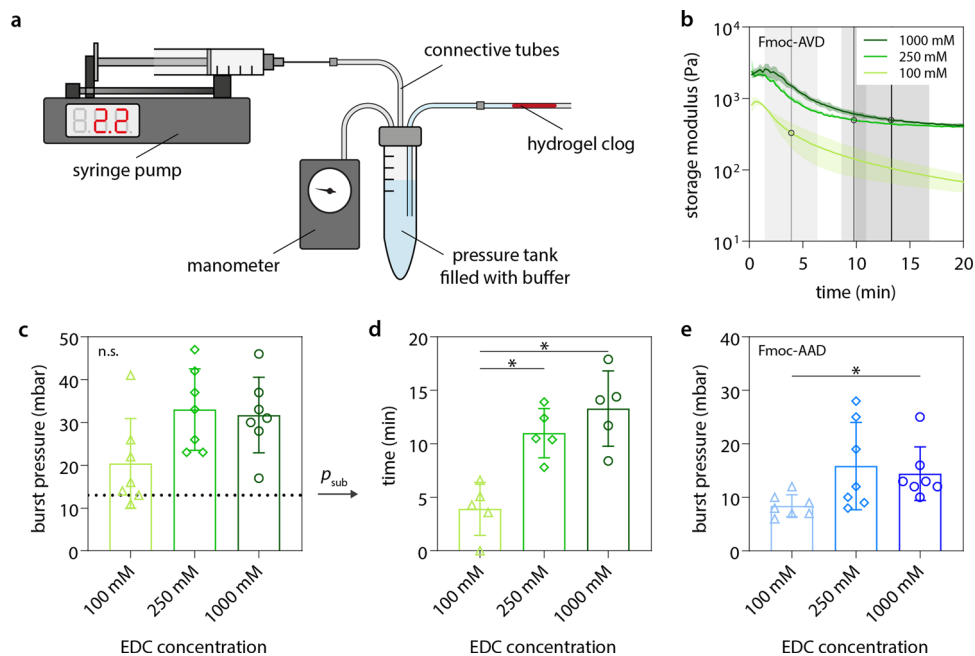


**Fig. 3 Transient clogging of tubings.** Schematic illustration of the fluidic system used to conduct the clogging experiments (a). The pressure resistance of clogs formed by Fmoc-AVD and Fmoc-AAD hydrogels in macroscopic tubings depends on the fuel concentration (c, e). If Fmoc-AVD hydrogel clogs are exposed to a subcritical pressure (black dashed line in c), they withstand this mechanical load for a certain, fuel-dependent time span (d). This time span reflects the time point in the gelation curves where the gel stiffness falls below a critical value (circles in b). Data shown represents the mean and the standard deviation as obtained from  $n = 3$  (b),  $n = 7$  (c, e), and  $n = 5$  (d) independent samples. The level for significance was set to  $p < 0.05$  and determined by ordinary one-way ANOVA and Tukey post hoc test (c, d) or Kruskal-Wallis test in combination with the Dunn's multiple comparisons test (e). Fmoc-AVD data is depicted in green and Fmoc-AAD data in blue. Bright colors represent an EDC concentration of 100 mM, medium bright colors correspond to 250 mM, and dark colors to 1000 mM. Individual data points are depicted with triangles (100 mM EDC), rhombuses (250 mM EDC), and circles (1000 mM).

further increasing the fuel concentration from 250 to 1000 mM has almost no impact on the maximum elasticity of the Fmoc-AVD system ( $G'_{1000} = 2.6 \pm 0.5$  kPa)—and similarly, also the pressure resistance of a Fmoc-AVD hydrogel clog generated with 250 mM fuel is not further enhanced when the amount of fuel is increased (Fig. 3c). With the measured burst pressure values and the peak values of the elastic moduli determined for the different hydrogel variants, we estimate critical strain levels (which correspond to the respective burst events) ranging between ~1 and 2% (Supplementary Results Section 1.2 and Supplementary Table 1). Those estimated critical strain values agree reasonably well with the results from the LAOS experiments, where we observed that the samples enter nonlinear behavior at those strain levels. In other words, this result implies that failure of the hydrogel clogs occurs as soon as the linear response regime of the material is left, i.e., when the hydrogels start to get damaged.

When using a dynamic hydrogel system for a clogging test as we conduct it here, the maximal elasticity of the hydrogel clog is not the only relevant parameter to consider; instead, the intrinsic lifetime of the gel can also be expected to contribute to the failure process of such a hydrogel clog. To test this notion, we next apply a subcritical pressure to the hydrogel clogs, i.e., a pressure level that is smaller than the burst pressure levels we determined above. When such a (constant) subcritical pressure level (here, selected 13 mbar) is applied to a Fmoc-AVD hydrogel clog fueled with 100 mM EDC, we observe clog failure after ~4–5 min (Fig. 3d). Using the time-dependent viscoelasticity properties determined before, we find that this time point corresponds to an elasticity range of  $G'_{\text{crit}} \sim 120\text{--}760$  Pa (Fig. 3b). With this result, we expect that the failure of the hydrogel clog should be delayed, when the fuel concentration is increased from 100 to 250 mM: At this higher fuel concentration, the lifetime of the hydrogel is

extended such that a similarly low level of hydrogel elasticity is not reached within the first 5 min. Indeed, failure of this hydrogel clog occurs a bit later, i.e., around ~11–12 min, which is in line with our expectation. Accordingly, another (yet small) increase in the clog lifetime is obtained when even larger amounts of fuel (i.e., 1000 mM EDC) are used (Fig. 3d). Also, this result is in good agreement with the time-dependent viscoelastic properties of this hydrogel variant, which requires even more time to soften up to levels in the range of a few hundreds of Pa (Fig. 3b).

When we use the same setup to test the pressure resistance of softer Fmoc-AAD-based gels, the obtained results are in good agreement with the viscoelastic properties of those gels as we discussed above. For instance, we observe that the burst pressure values we determine for such Fmoc-AAD clogs only weakly depends on the fuel concentration used to generate those hydrogels. Similar to the maximal shear moduli determined in the linear response regime, this burst pressure only increases when the fuel concentration is increased from 100 mM to 250 mM—but not beyond that (Fig. 3e). Also here, based on the measured burst pressures, we estimate a critical strain of ~1–2% (Supplementary Table 1) upon which clog failure is triggered—and this critical strain level agrees well with the LAOS measurements we described for those Fmoc-AAD hydrogels above. In other words, all hydrogel clog variants fail at such conditions where the linear response regime ends. Here, the hydrogels can no longer withstand the mechanical load they are exposed to; depending on the measuring setup used, this results in either strain weakening or clog failure.

**Influence of reaction waste products on the hydrogel lifetime.** So far, we have discussed the influence of mechanical load and the intrinsic lifetime of the dynamic hydrogels on the viscoelastic

properties of the self-assembled materials. As mentioned above, increasing the fuel concentration from 250 to 1000 mM neither increases the maximal stiffness of the hydrogels nor their intrinsic lifetime. Based on this result, one might assume that 250 mM of fuel is sufficient to generate the highest anhydride concentration possible—at least for a short time period. This idea would be consistent with our observation that the Fmoc-systems fueled with this particular EDC concentration show a similarly high maximal elastic modulus as the same system fueled with 1000 mM EDC. However, as the cyclic EDC conversion reaction drives the assembly process of the Fmoc-conjugates, any excess EDC molecules should be able to immediately reactivate the hydrolyzed (and thus disassembling) variants of the Fmoc-anhydrides. As a consequence, hydrogel samples containing 1000 mM fuel should show a prolonged regime where a near-to-maximal elastic modulus is present. Why is this not the case?

The EDC-based reaction cycle is rather simple, and the only molecular component we neglected in our considerations so far is the reaction waste product EDU (Fig. 4a). One possible explanation as to why larger EDC concentrations return unexpected results could be that an accumulation of this “waste” product within the sample might negatively affect the ongoing conversion reaction of the Fmoc-precursors to the anhydride. To test this idea, we add 1000 mM EDU to a Fmoc-AVD sample (which already contains 1000 mM EDC) and again track the development of its viscoelastic properties. Interestingly, the presence of EDU seems to prevent the formation of a hydrogel: the system now remains dominated by its viscous properties, and we do not detect any sign of gelation (Fig. 4b).

To obtain a better understanding of how EDU might interact with the microscopic mechanism of the self-assembling system, we choose two additional molecules, which mimic different parts of the chemical structure of EDU: First, urea—this molecule is selected to mimic the urea group of EDU. Second, methyl 3-(dimethylamino)propionate (MDP)—at the pH value used for our experiments, MDP contains a slightly hydrophobic and positively charged carbon chain, which approximates the carbon chain of EDU (Fig. 4a). In the aqueous environment used here, the hydrolysis of the ester MDP into its carboxylic acid and methanol is rather slow (Supplementary Results Section 1.3 and Supplementary Fig. 5); thus, such an MPD hydrolysis should not significantly impact our experiments. When we add one of those two EDU-mimetics, i.e., urea or MDP, to the same Fmoc-AVD sample tested before, we obtain the following results: Whereas even high concentrations of urea (i.e., 3000 mM) do not affect the gelation process of Fmoc-AVD at all, the presence of MDP prevents gelation (Fig. 4b).

Together, those results suggest that the carbon chain of EDU (or MDP) interacts with the Fmoc-system such that its self-assembly process is disturbed. At this point, it is important to recall that the carbon chains of both, EDU and MDP, combine hydrophobic as well as cationic properties, and the latter originate from the tertiary amine groups present in the molecules. Thus, EDU, as well as MDP, could interact with the Fmoc-conjugates via cation- $\pi$  interactions between these tertiary amine groups of MDP/EDU and the Fmoc-group, and/or via electrostatic interactions between the tertiary amine groups of MDP/EDU and the anionic carboxyl group of the Fmoc-precursor. Either of those interactions could disturb the self-assembly process of the system and inhibit the formation of fibers and thus hydrogels.

Of course, the conditions we created for this particular set of tests, i.e., mixing the precursor with both, fuel and waste molecules, do not correctly reproduce the scenario present in the dynamically self-assembling gels: here, at the beginning of the experiment, the concentration of waste molecules is close to zero but increases over time while the reaction cycle converts EDC. To

better mimic this dynamic scenario, we change the setting of our rheological measurements. In detail, we switch to a custom-made setup, where we can expose a preformed hydrogel to waste molecules *in situ*<sup>42</sup> (see the schematic in Fig. 4c and the Methods section “Measurements with a perforated plate setup” for technical details). As this complex setup can have small influences on the absolute values of the measured viscoelastic moduli, we first set a new baseline by again measuring the gelation behavior of Fmoc-AVD samples without the addition of any interfering agents. Overall, as expected, the time-dependent behavior of the chemically fueled hydrogels is successfully reproduced (Supplementary Results Section 1.4 and Supplementary Fig. 6). Then, once more, we observe the gelation behavior of a Fmoc-AVD hydrogel fueled with 1000 mM EDC; however, this time, the fluid chamber is filled with only 1000 mM EDC dissolved in 200 mM 2-(*N*-morpholino)ethanesulfonic acid (MES) buffer at the beginning of this measurement. After recording the viscoelastic properties of the sample for 20 min (the corresponding time point is indicated by the red dashed line in Fig. 4d), the fluid in the reservoir is replaced with a solution containing 1000 mM MDP in addition to 1000 mM EDC.

Interestingly, for the preformed Fmoc-AVD hydrogel, this exposure to MDP only results in a small measuring artifact, which is created by a sudden increase in pressure in the reservoir chamber (this pressure increase is generated when the pump is started to exchange the fluid in this reservoir). In contrast, for Fmoc-AAD hydrogels, similar sudden exposure to MDP does affect the viscoelastic properties of the system. Here, after observing a similar artifact induced by the buffer exchange process (which is more strongly pronounced for the softer Fmoc-AAD hydrogel than for the stiffer Fmoc-AVD gel), we detect full liquefaction of the system: in other words, the system returns into its liquid state that is dominated by the loss modulus (Fig. 4f). This difference in the hydrogel behavior is very interesting as an immediate exposure of Fmoc-AAD conjugates to EDU, urea, or MDP prior to gel formation returns virtually identical results (Fig. 4e) as what we described for Fmoc-AVD above. Consistently, a preformed Fmoc-AVD gel maintains its supramolecular structures upon MDP addition: here, the sample turbidity persists after MPD addition, and confocal microscopy images show similar supramolecular structures as in the absence of MDP (Fig. 4g). In contrast, just minutes after MDP was added to the test tube, turbid Fmoc-AAD gels are reverted into clear samples. Accordingly, fluorescent images obtained for such MDP-enriched Fmoc-AAD systems show the disintegration of the previously present supramolecular structures (Fig. 4h). To visualize the dynamic structural changes in the gels, time-lapse movies (Supplementary Movies 1–4) of both peptide systems with and without the addition of MDP were obtained using confocal microscopy (those are available as electronic SI). To quantify the turbidity of the gels, light absorption measurements were conducted. Also here, the gels are initially turbid indicating a successfully formed gel structure (Supplementary Results Section 1.5 and Supplementary Fig. 7a–f). Upon addition of MDP, we observe a loss of turbidity for preformed gels generated from Fmoc-AAD, but not for those generated from Fmoc-AVD (Supplementary Fig. 7g, h).

Together, we interpret those results as follows: As mentioned above, hydrophobic attractive forces are responsible for driving the self-assembly of both variants of Fmoc-conjugates into supramolecular structures and, consequently, the formation of macroscopic hydrogels. When the Fmoc-derivates are brought into contact with the waste product EDU prior to gelation, the EDU molecules might bind to (and thus shield) the hydrophobic domains of the anhydride thus preventing self-assembly. Yet, when the Fmoc-derivates are already present in their self-

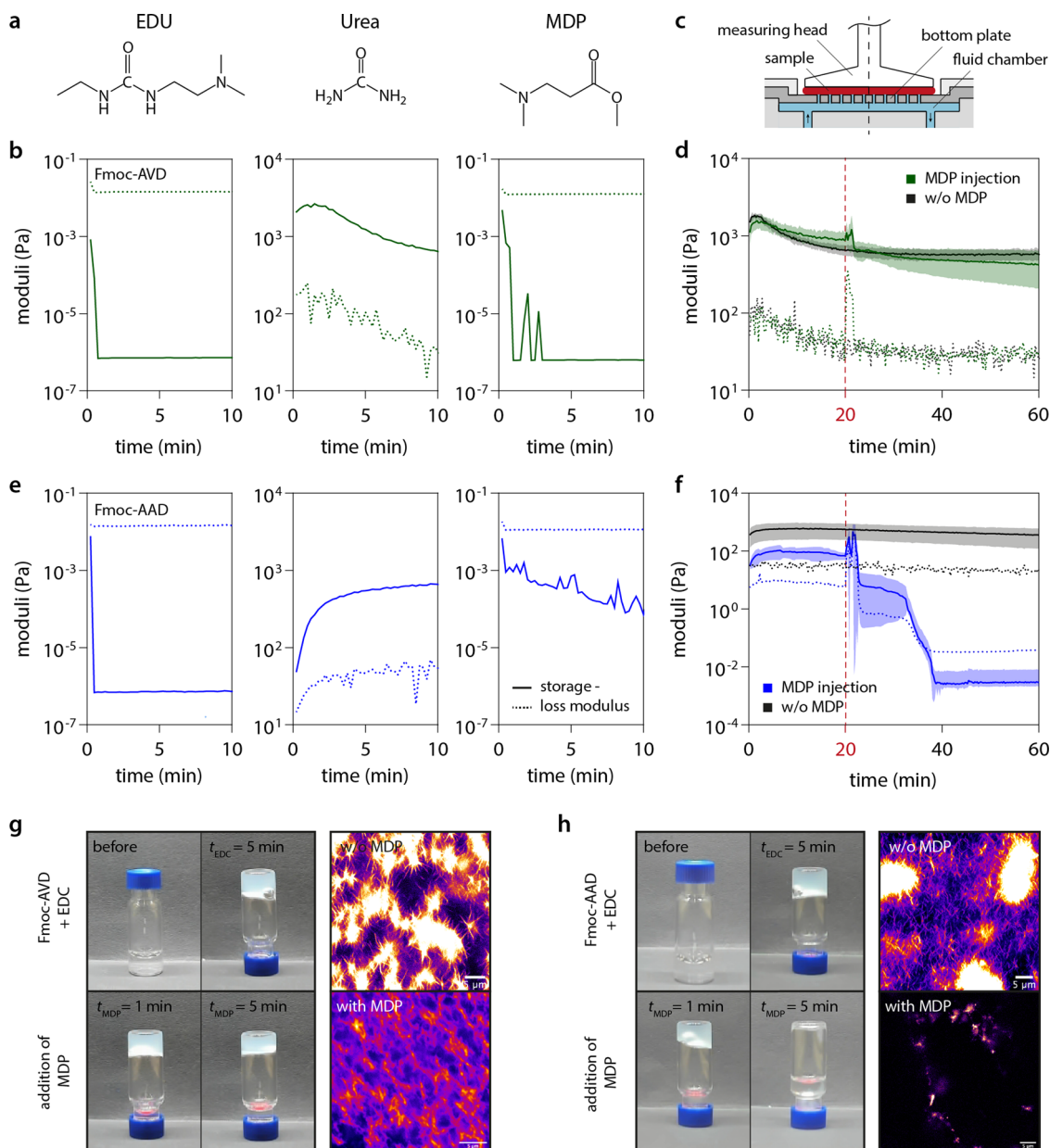


**Fig. 4** Influence of reaction side products on the viscoelastic properties of chemically fueled hydrogels. The waste product of the reaction cycle (EDU) and its structural mimetics (a) affect the gelation behavior of Fmoc-AVD (green) and Fmoc-AAD (blue) differently (b, e). Custom-made rheological setup to assess the behavior of preformed gels when brought into contact with the waste-mimetic MDP (c): here, the viscoelastic properties of a preformed Fmoc-AVD gel exposed to MDP after 20 min (dashed red line) remain virtually unaffected (d). However, a preformed Fmoc-AAD gel disintegrates upon exposure to MDP (f). Reference measurements without the addition of MDP are illustrated in gray for both peptide systems. Data shown represents the mean as obtained from  $n \geq 3$  independent samples. Error bands (d, f) depict the standard deviation. Inverted tube tests and fluorescent imaging of Fmoc-AVD (g) and Fmoc-AAD (h) samples further illustrate gel formation and gel (in)stability after MDP addition.

assembled state (e.g., as fibers) the strength of the stabilizing interactions determines if those supramolecular structures can be disintegrated by EDU. Based on the molecular architecture of the tripeptides conjugated to the Fmoc-groups, it is reasonable to assume that the hydrophobic forces responsible for self-assembly are weaker for Fmoc-AAD than for Fmoc-AVD. Thus, preformed Fmoc-AAD gels are more sensitive to EDU addition than Fmoc-AVD, which is why the former liquefy and the latter do not.

For other, less dynamic hydrogel systems, similar effects of molecular additives on the gel properties were observed previously and were used to adjust the gel properties in a controlled manner<sup>43,44</sup>. Owing to their ability to aggregate in water and to interact with hydrophobic gel structures,

hydrophobic additives are especially well suited for this purpose. For instance, by adding poly(lactic acid) it is possible to generate porous hydrogels<sup>45</sup>, and the swelling behavior of certain gel systems can be modified by the addition of hydrophobic additives such as benzoic acid or phenol<sup>46</sup>. Moreover, using molecular additives, the viscoelastic properties of hydrogels can be tuned: when poly(ethylene glycol) is added to poly(vinyl pyrrolidone) hydrogels, this reduces the gel stiffness; in contrast, the addition of poly(ethylene oxide) increases the elasticity of this gel variant<sup>47</sup>. In addition to affecting the lifetime of self-assembling peptide systems as we demonstrate here, such other molecular additives could be used in the future to further tailor the properties of chemically fueled hydrogels.



## Conclusions

We demonstrate that the chemically fueled peptide conjugates Fmoc-AVD and Fmoc-AAD offer tunable mechanical properties both in the linear and nonlinear response regime. In addition, we demonstrate that the lifetime of the emerging supramolecular materials depends not only on the amount of fuel available for creating assembly-competent molecules but also on the concentration of accumulated waste products, which can destabilize the assembled structures. Future developments of this class of materials have to take this additional parameter into account when designing molecular features of the self-assembling Fmoc-peptides. In brief, such dynamic hydrogels do not only come with intrinsic, preprogrammed material properties, they also allow for externally influencing the lifetime of the self-assembled structures. The possibility to combine adjustable mechanical properties with an a priori programmable and a posteriori tunable lifetime opens up a broad range of future applications for such dynamic materials: we expect that similar systems could be used as pre-programmable sealings for (micro)-fluidic systems, or as components in soft actuators and micro-robotics.

## Materials and methods

**Chemicals.** The following commercial chemicals were used for the synthesis of the Fmoc-tripeptides: deuterated dimethyl sulfoxide (DMSO- $d_6$ ), *N*, *N'*-diisopropylcarbodiimide (DIC), ethyl (hydroxyimino)cyanoacetate (oxyma) (Novabiochem<sup>®</sup>), piperidine (99%), protected amino acids alanine (Fmoc-A-OH) and valine (Fmoc-V-OH), solvents (acetonitrile (ACN), *N*, *N*-dimethylformamide (DMF), dichloromethane, double distilled water (MilliQ<sup>®</sup> Direct 8), trifluoroacetic acid (99%, TFA), triisopropylsilane (TIPS), and preloaded Fmoc-Asp(OtBu)-Wang resin (100–200 mesh, loading 0.67 mmol  $g^{-1}$ ). The chemicals were purchased from Sigma-Aldrich (St. Louis, USA) and used without any further purification unless indicated otherwise. For the rheological measurements, the hydrogel clog tests in tubings, the inverted tube tests, and confocal microscopy, the following commercial chemicals were used: 1-ethyl-3-(3-dimethylaminopropyl)carbodiimid-hydrochlorid (EDC) (Carl Roth GmbH + Co. KG, Karlsruhe, Germany), 1-[3-(dimethylamino)propyl]-3-ethylurea (EDU) (Alfa Aesar, Ward Hill, USA), Urea (Carl Roth GmbH + Co. KG), methyl 3-(dimethylamino)propionate (MDP) (Sigma-Aldrich, St. Louis, USA). For the confocal microscopy, additionally, the dye Nile red (Sigma-Aldrich, St. Louis, USA) was used.

**Peptide synthesis and purification.** Peptides were synthesized using standard fluoren-9-ylmethoxycarbonyl (Fmoc) solid-phase peptide synthesis on preloaded Fmoc-Asp(OtBu)-Wang resin (100–200 mesh, loading 0.67 mmol  $g^{-1}$ ). Peptide synthesis was conducted on a 0.5 mmol scale using a CEM Liberty microwave-assisted peptide synthesizer, and the Liberty Blue Application Software (Copyright © CEM Corporation 2015, Version: 1.45.5794.20265). Preloaded Fmoc-Asp(OtBu)-Wang resin (100–200 mesh, loading 0.67 mmol  $g^{-1}$ ) was swelled 30 min in 10 mL DMF at room temperature. Next, the preloaded Fmoc-Asp(OtBu)-Wang resin (100–200 mesh, loading 0.67 mmol  $g^{-1}$ ) was put into the automated peptide synthesizer. Before the following amino acid-coupling, a 20% (v/v) solution of piperidine (1 × 10 mL) in DMF was used to remove the *N*-terminal Fmoc protecting group. The reaction mixture was heated in the microwave (1 × min, 90 °C). This step was repeated. Next, the resin was washed with DMF (2 × 10 mL). The coupling was achieved by using four equivalents (eq.) of Fmoc-V-OH respectively Fmoc-A-OH in DMF (0.2 M, 10 mL), 4 eq. of DIC (0.5 M, 4 mL), and 4 eq. of oxyma (1 M, 2 mL). This resin solution was heated in the microwave (1 × min, 90 °C). To increase the yield, this amino acid coupling step was repeated. After the two coupling steps, the resin was washed with DMF (2 × 10 mL). The 2 × Fmoc-deprotection, washing, 2 × coupling, the washing cycle was carried out to couple also the last amino acid Fmoc-A-OH of the respective peptide sequence Fmoc-alanine-valine-aspartic acid (AVD), and Fmoc-alanine-alanine-aspartic acid (AAD), respectively. Then, the peptide was cleaved from the resin by reacting the resin with a solution of 2.5% MQ-water, 2.5% TIPS, and 95% TFA for 1 h under continuous agitation at room temperature. Rotary evaporation by co-distillation with dichloromethane removed the solvent, and the crude product was dried under reduced pressure. Next, the crude peptides Fmoc-AVD and Fmoc-AAD were dissolved in ±50% acetonitrile in MQ-water and then purified using reversed-phase high-performance liquid chromatography (RP-HPLC, Thermo Fisher Dionex Ultimate 3000, Hypersil Gold 5  $\mu$ m, length 250 mm, ID 20 mm.) with gradient elution from 40 to 98% acetonitrile (with 0.1% TFA) in MQ-water (with 0.1% TFA) and a flow rate of 20 mL/min. UV-Vis detection at 254 nm was applied to detect the peptide. The purified peptide was lyophilized (Lyophilyle: Alpha LDplus, Christ) and stored at –20 °C until further use. <sup>1</sup>H-NMR spectroscopy (Supplementary Results Section 1.6 and Supplementary Fig. 8), Electrospray ionization mass spectrometry (ESI-MS, positive mode) on an LCQ

Fleet Ion Trap Mass Spectrometer (Thermo Scientific, Supplementary Table 2), as well as analytical HPLC (ThermoFisher Dionex Ultimate 3000, Hypersil Gold, Diameter (mm) 250 × 4.6), eluted with a gradient of 0.1% TFA in MQ-water: ACN from 98:2 to 2:98 in 14 min. (Supplementary Fig. 9) was used to analyze the purity of the peptides Fmoc-AVD and Fmoc-AAD. <sup>1</sup>H-NMR spectra were recorded on a Bruker 500 MHz NMR. Chemical shifts are reported as  $\delta$ -values in parts per million (ppm) relative to the deuterated solvent peak: DMSO- $d_6$  ( $\delta$ H: 2.50). For the denotation of the observed signal multiplicities, the following abbreviations were used: d (doublet), dd (doublet of doublets), and m (multiplet).

## Rheological characterizations

**Gelation tests.** To determine the gelation behavior of the hydrogels<sup>48</sup>, rheological measurements were performed using a commercial shear rheometer (MCR 302, Anton Paar, Graz, Austria) and a plate-plate geometry (bottom plate: P-PTD 200/AIR, Anton Paar; 25 mm steel measuring head: PP25, 79044, Anton Paar). The sample volume was 200  $\mu$ L for each measurement; the plate separation was set to 0.3 mm and kept constant during all measurements. A solvent trap (a chamber containing a water-soaked paper towel, covered with a lid), as well as temperature control of the bottom plate (set to 21 °C), was used for all measurements. With this configuration, sample dehydration can be avoided for up to 6 h (Supplementary Results Section 1.7 and Supplementary Fig. 10).

To obtain the gels, the first 50  $\mu$ L of an EDC stock solution ( $c_{EDC} = 400, 1000,$  or 4000 mM solubilized in 200 mM MES, pH = 6) was homogeneously spread onto the bottom plate of the rheometer; then 150  $\mu$ L of the respective Fmoc-conjugate solution ( $c_{Fmoc} = 13.3$  mM, solubilized in 200 mM MES, pH = 6) was added on top. No further mixing was conducted to ensure that structures self-assembling in situ were not disrupted. With this method, the gels do not need to be transferred, which minimizes mechanical perturbation prior to their characterization. Then, the measuring head was lowered, and the test was started immediately afterwards. To ensure linear material response during the gelation process of the samples, the measurements were performed in torque-controlled mode (by applying small torques of 0.5  $\mu$ Nm and a constant oscillation frequency of 1 Hz). The storage and loss moduli were determined for at least 30 min, and one measurement point was recorded every 15 s. For determining the influence of EDU, urea, and MDP on the gelation behavior of the Fmoc-samples, the respective substance was added to the EDC stock solution (here, always  $c_{EDC} = 4000$  mM in 200 mM MES, pH = 6; then, either:  $c_{EDU} = 4000$  mM, or  $c_{urea} = 12000$  mM, or  $c_{MDP} = 4000$  mM) and the procedure was conducted the same way as described above. For urea, a high concentration, close to the limit of solubility (1200  $g L^{-1}$ , Haynes 2016<sup>49</sup>) was tested to see if it has an effect on the gelation behavior at all. For each sample type, three independent samples were created and characterized in situ.

**LAOS measurements.** For assessing the onset of nonlinear material response, LAOS experiments were performed using the same setup and sample preparation protocol as described above. As LAOS tests slowly but steadily increase the applied shear strain, they are well suitable to investigate the nonlinear behavior of viscoelastic solids such as the hydrogels used here. At the same time, since LAOS makes use of an oscillatory strain application, it is still possible to determine the storage modulus and loss modulus as well as the point where material failure takes place. The linear elastic regime is valid for small strains only. In this regime, Hooke's law applies and a linear relation between stress and strain is observed. At larger mechanical loads, either strain weakening or strain hardening sets in<sup>50</sup> and Hooke's law is not valid anymore. The storage and loss moduli were determined in strain-controlled mode, and the applied shear strain was increased logarithmically from 0.1 to 1000% (using a constant oscillation frequency of 1 Hz and collecting two data points in each strain decade). For all Fmoc-AVD samples, the tests were started immediately after the samples were placed on the bottom plate; this was necessary as those samples reach their maximal stiffness quite rapidly after the different molecular components are brought together. In contrast, the Fmoc-AAD samples were allowed to rest for 3 min after the components were brought together; here, this was necessary since those samples require ~3 min to reach their maximal stiffness (this was determined in the gelation measurements, which were conducted prior to the LAOS tests). For each sample type, three independent samples were created and characterized in situ.

**Measurements with a perforated plate setup.** To test the effect of MDP on preformed hydrogels, a custom-made rheological setup was used; this setup allows for bringing the sample in contact with a liquid reservoir located below the sample plane (Fig. 4c). This dedicated setup was enabled in the same commercial shear rheometer (MCR 302, Anton Paar) used for the other tests; also here, a commercial measuring head (PP25, 79044, Anton Paar) was employed. Yet, an in-house developed, perforated bottom plate (from now on referred to as "hole-y plate") and first described in Yan et al., 2019<sup>42</sup> was used. This hole-y plate can be mounted onto the commercial bottom plate of the rheometer (P-PTD200/80-I, Anton Paar) and comprises 19 regularly orientated holes with a diameter of 1.5 mm each. This design allows fluid to diffuse from a reservoir chamber located below the measurement gap into the actual sample. The sample and the reservoir of the hole-y plate were separated by a polycarbonate membrane (Whatman Nuclepore track-etch membrane, pore size: 50 nm, GE Healthcare, Chalfont St Giles, Great Britain) to prevent the sample from leaking into the fluid chamber while allowing small



molecules (such as EDU or MDP) to penetrate the membrane and to enter the sample.

First tests without the addition of MDP were conducted to validate the measurement setup. Before the measurement, the reservoir was filled with 200 mM MES buffer (pH 6) containing the same EDC concentration as of the investigated Fmoc-based sample (i.e.,  $c_{\text{EDC}} = 100, 250, \text{ or } 1000 \text{ mM}$ ). For these tests, the inlet and outlet of the chamber was closed, so that no additional fluid exchange is possible, and the sample interacts only with the static reservoir. In the next step, the inlet and outlet of the fluid chamber was used for the addition of MDP ( $c_{\text{MDP}} = 1000 \text{ mM}$  added to 200 mM MES containing 1000 mM EDC, pH 6) by using a syringe pump (LA 100, Landgraf Laborsysteme HLL GmbH, Langenhagen, Germany) after the sample has formed a gel. Here only the highest EDC concentration was investigated, resulting in the most stable gel. In all cases, sample preparation on top of the membrane was conducted in the same way as described for the gelation experiments above. Furthermore, the same measurement parameters as during the standard gelation tests were applied. Only the solvent trap could not be used in this setup, due to the inlet and outlet of the hole-y plate. Here, the liquid reservoir prevents the draining of the samples. For each sample type, three independent samples were created and characterized in situ.

**Confocal fluorescence microscopy.** Confocal fluorescence microscopy was performed with a Leica TCS SP8 confocal microscope using a 63x water immersion objective with a numerical aperture of 1.2. Samples with a total reaction volume of 20  $\mu\text{L}$  were prepared directly in an ibidi  $\mu$ -slide angiogenesis well plate. About 25  $\mu\text{M}$  Nile red was added as a dye before the fuel EDC was added. Samples were excited with a 552 nm laser and imaged at 577–656 nm. A laser intensity of 0.3 or 1.0%, and a pinhole of either 23.92, 39.61, 79.22, or 111.3  $\mu\text{m}$  ( $\lambda_{\text{emission}} = 580 \text{ nm}$ ) was used to image the samples. The software ImageJ 1.52p (Java 1.80\_172, 64-bit) was used to analyze all recorded images. Imaging was conducted at 22 °C.

**Macroscopic images of gels.** Samples of 10 mM Fmoc-AAD/ 10 mM Fmoc-AVD with a total reaction volume of 500  $\mu\text{L}$  were prepared in 1.5 mL screw cap HPLC vials. The samples were imaged after EDC addition with a high-definition camera.

**Transient clogging of fluidic systems.** To test the ability of the self-assembled hydrogels to transiently clog a tubing, we used a custom-made setup, which comprises a syringe pump (LA 100, Landgraf Laborsysteme HLL GmbH, Langenhagen, Germany) and a small pressure regulation tank. In combination, those two items allowed for applying a controlled pressure onto a fluid-filled outlet tube. Furthermore, a manometer (GDH 13 AN, Greisinger Electronic GmbH, Regenstauf, Germany) was attached to the pressure tank to monitor the pressure in the system. The outlet tube comprised an exchangeable, 10 cm long silicon test tube (inner diameter = 1 mm, Rotilabo, Carl Roth, Karlsruhe, Germany) which was intentionally clogged in the experiments (Fig. 3a). To generate such a clog, 60  $\mu\text{L}$  of a Fmoc-peptide solution ( $c_{\text{AVD}} = c_{\text{AAD}} = 13.3 \text{ mM}$  in 200 mM MES pH = 6) and 20  $\mu\text{L}$  of an EDC solution ( $c_{\text{EDC}} = 400, 1000, \text{ or } 4000 \text{ mM}$ ; all solutions were prepared in 200 mM MES at pH = 6) were combined using a 100  $\mu\text{L}$  Hamilton syringe and immediately injected into the outlet tube. The hydrogel clog was then allowed to form in situ and was left to rest for 90 s to ensure that the system reaches its maximal mechanical stability. Then, an increasing pressure was applied (at a rate of 1 mbar/s) to this hydrogel clog until it failed; the corresponding pressure level at which this clog failure occurred is referred to as “burst pressure” in the main text. To test the stability of a hydrogel clog in the presence of constant, subcritical pressure, a pressure level of 14 mbar was selected and applied to the clog; then, the time point was determined at which the hydrogel clog failed.

**Data analysis.** Prior to statistical analysis, we tested for the normal distribution of the measured values by using the Shapiro–Wilk test. To detect statistical differences between more than two groups, ordinary one-way ANOVA (for normally distributed samples) and Kruskal–Wallis test (for non-normal distribution) were conducted. Multi-comparisons were performed using the Tukey post hoc test or the Dunn’s multiple comparisons test, respectively. Professional software (Prism 8, GraphPad Software, San Diego, CA, USA) was used to conduct all statistical calculations. The level for the significant difference was set to  $p < 0.05$ , and significant differences were marked with an asterisk where applicable. Where no significant difference was found, the abbreviation n.s. was used.

## Data availability

The authors declare that the experimental and theoretical data supporting the findings of this study are available within the paper (and its supplementary information files). However, more data that support the findings of this study are available from the corresponding authors upon reasonable request.

Received: 22 April 2021; Accepted: 1 September 2021;

Published online: 17 September 2021

## References

- Philp, D. & Stoddart, J. F. Self-assembly in natural and unnatural systems. *Angew. Chem. Int. Ed.* **35**, 1154–1196 (1996).
- Fialkowski, M. et al. Principles and implementations of dissipative (dynamic) self-assembly. *J. Phys. Chem. B* **110**, 2482–2496 (2006).
- Honorato-Rios, C. & Lagerwall, J. P. F. Interrogating helical nanorod self-assembly with fractionated cellulose nanocrystal suspensions. *Commun. Mater.* **1**, 1–11 (2020).
- Freeman, R. et al. Reversible self-assembly of superstructured networks. *Science* **362**, 808–813 (2018).
- Sutar, P. et al. Binder driven self-assembly of metal-organic cubes towards functional hydrogels. *Nat. Commun.* **9**, 1–12 (2018).
- Hua, M. et al. Strong tough hydrogels via the synergy of freeze-casting and salting out. *Nature* **590**, 594–599 (2021).
- Panja, S. & Adams, D. J. Gel to gel transitions by dynamic self-assembly. *Chem. Commun.* **55**, 10154–10157 (2019).
- Panja, S., Patterson, C. & Adams, D. J. Temporally-programmed transient supramolecular gels. *Macromol. Rapid Commun.* **40**, 1900251 (2019).
- Singh, N. et al. Devising synthetic reaction cycles for dissipative nonequilibrium self-assembly. *Adv. Mater.* **32**, 1906834 (2020).
- Astumian, R. D. Kinetics asymmetry allows macromolecular catalysts to drive an information ratchet. *Nat. Commun.* **10**, 1–14 (2019).
- Pezzato, C. & Prins, L. J. Transient signal generation in a self-assembled nanosystem fueled by ATP. *Nat. Commun.* **6**, 1–8 (2015).
- te Brinke, E. et al. Dissipative adaptation in driven self-assembly leading to self-dividing fibrils. *Nat. Nanotechnol.* **13**, 849–855 (2018).
- Maiti, S. et al. Dissipative self-assembly of vesicular nanoreactors. *Nat. Chem.* **8**, 725–731 (2016).
- Dhiman, S., Jain, A. & George, S. J. Transient helicity: Fuel-driven temporal control over conformational switching in a supramolecular polymer. *Angew. Chem. Int. Ed.* **129**, 1349–1353 (2016).
- De, S. & Klajn, R. Dissipative self-assembly driven by the consumption of chemical fuels. *Adv. Mater.* **30**, 1706750 (2018).
- della Sala, F. et al. Transient self-assembly of molecular nanostructures driven by chemical fuels. *Curr. Opin. Biotechnol.* **46**, 27–33 (2017).
- Zhang, B. et al. Chemically fueled covalent crosslinking of polymer materials. *Chem. Commun.* **55**, 2086–2089 (2019).
- Wang, G. & Liu, S. Strategies to construct a chemical-fuel-driven self-assembly. *ChemSystemsChem* **2**, e1900046 (2020).
- Ragazzon, G. & Prins, L. J. Energy consumption in chemical fuel-driven self-assembly. *Nat. Nanotechnol.* **13**, 882–889 (2018).
- Leira-Iglesias, J. et al. Oscillations, travelling fronts and patterns in a supramolecular system. *Nat. Nanotechnol.* **13**, 1021–1027 (2018).
- Singh, N. et al. Re-programming hydrogel properties using a fuel-driven reaction cycle. *J. Am. Chem. Soc.* **142**, 4083–4087 (2020).
- Falzone, T. T. et al. Assembly kinetics determine the architecture of  $\alpha$ -actinin crosslinked F-actin networks. *Nat. Commun.* **3**, 1–9 (2012).
- Levin, M. et al. Kinetics of actin networks formation measured by time resolved particle-tracking microrheology. *Soft Matter* **16**, 7869–7876 (2020).
- Deshpande, S. & Pfohl, T. Hierarchical self-assembly of actin in micro-confinements using microfluidics. *Biomicrofluidics* **6**, 034120 (2012).
- Boekhoven, J. et al. Dissipative self-assembly of a molecular gelator by using a chemical fuel. *Angew. Chem. Int. Ed.* **122**, 4935–4938 (2010).
- Hao, X. et al. Pulsating polymer micelles via ATP-fueled dissipative self-assembly. *ACS Macro Lett.* **6**, 1151–1155 (2017).
- Wood, C. S. et al. Fuel-controlled reassembly of metal–organic architectures. *ACS Cent. Sci.* **1**, 504–509 (2015).
- Del Grosso, E. et al. Dissipative synthetic DNA-based receptors for the transient loading and release of molecular cargo. *Angew. Chem. Int. Ed.* **57**, 10489–10493 (2018).
- Tena-Solsona, M. et al. Non-equilibrium dissipative supramolecular materials with a tunable lifetime. *Nat. Commun.* **8**, 1–8 (2017).
- Rieß, B., Grötsch, R. K. & Boekhoven, J. The design of dissipative molecular assemblies driven by chemical reaction cycles. *Chem* **6**, 552–578 (2020).
- Sorrenti, A. et al. Non-equilibrium steady states in supramolecular polymerization. *Nat. Commun.* **8**, 1–8 (2017).
- Dai, K. et al. Regulating chemically fueled peptide assemblies by molecular design. *J. Am. Chem. Soc.* **142**, 14142–14149 (2020).
- Orbach, R. et al. The rheological and structural properties of Fmoc-peptide-based hydrogels: the effect of aromatic molecular architecture on self-assembly and physical characteristics. *Langmuir* **28**, 2015–2022 (2012).
- Adams, D. J. et al. Relationship between molecular structure, gelation behaviour and gel properties of Fmoc-dipeptides. *Soft Matter* **6**, 1971–1980 (2010).
- Rieß, B. et al. Dissipative assemblies that inhibit their deactivation. *Soft Matter* **14**, 4852–4859 (2018).
- Wanzke, C. et al. Dynamic vesicles formed by dissipative self-assembly. *ChemSystemsChem* **2**, e1900044 (2020).

37. Tena-Solsona, M. et al. Accelerated ripening in chemically fueled emulsions. *ChemSystemsChem* **3**, e2000034 (2021).
38. Wanzke, C. et al. Active droplets in a hydrogel release drugs with a constant and tunable rate. *Mater. Horiz.* **7**, 1397–1403 (2020).
39. Späth, F. et al. Molecular design of chemically fueled peptide–polyelectrolyte coacervate-based assemblies. *J. Am. Chem. Soc.* **143**, 4782–4789 (2021).
40. Donau, C. et al. Active coacervate droplets as a model for membraneless organelles and protocells. *Nat. Commun.* **11**, 1–10 (2020).
41. Kriebisch, B. A. K. et al. Reciprocal coupling in chemically fueled assembly: a reaction cycle regulates self-assembly and vice versa. *J. Am. Chem. Soc.* **142**, 20837–20844 (2020).
42. Yan, H. et al. Immune-informed mucin hydrogels evade fibrotic foreign body response in vivo. *Adv. Funct. Mater.* **29**, 1902581 (2019).
43. Mishra, G. P., Tamboli, V. & Mitra, A. K. Effect of hydrophobic and hydrophilic additives on sol–gel transition and release behavior of timolol maleate from polycaprolactone-based hydrogel. *Colloid Polym. Sci.* **289**, 1553–1562 (2011).
44. Semmling, B. et al. Development of hydrophobized alginate hydrogels for the vessel-simulating flow-through cell and their usage for biorelevant drug-eluting stent testing. *AAPS PharmSciTech* **14**, 1209–1218 (2013).
45. Zhang, X.-Z., Chu, C.-C. & Zhuo, R.-X. Using hydrophobic additive as pore-forming agent to prepare macroporous PNIPAAm hydrogels. *J. Polym. Sci. A Polym. Chem.* **43**, 5490–5497 (2005).
46. Koga, S., Sasaki, S. & Maeda, H. Effect of hydrophobic substances on the volume-phase transition of N-isopropylacrylamide gels. *J. Phys. Chem. B* **105**, 4105–4110 (2001).
47. Lugão, A. B., Rogero, S. O. & Malmonge, S. M. Rheological behaviour of irradiated wound dressing poly(vinyl pyrrolidone) hydrogels. *Radiat. Phys. Chem.* **63**, 543–546 (2002).
48. Schnitter, F. et al. Synthesis and characterization of chemically fueled supramolecular materials driven by carbodiimide-based fuels. *Nat. Protoc.* **16**, 3901–3932 (2021).
49. Haynes, W. M. *CRC handbook of chemistry and physics* (Taylor & Francis Group, LLC., 2017).
50. Lieleg, O. & Bausch, A. R. Cross-linker unbinding and self-similarity in bundled cytoskeletal networks. *Phys. Rev. Lett.* **99**, 158105 (2007).

## Acknowledgements

This project was funded by the Deutsche Forschungsgemeinschaft (DFG, German Research Foundation)—SFB 863, Projekt B11—111166240. The authors thank Marvin Ertel for helpful discussions regarding the structure of EDU mimetics. B.A.K.K. is grateful for a Kekulé Stipendium by the Verband der Chemischen Industrie.

## Author contributions

M.K., B.W., B.A.K.K., J.B. and O.L. planned the experiments, which were conducted and analyzed by M.K., B.W. and B.A.K.K. The manuscript was written by contributions of all authors.

## Funding

Open Access funding enabled and organized by Projekt DEAL.

## Competing interests

The authors declare no competing interest.

## Additional information

**Supplementary information** The online version contains supplementary material available at <https://doi.org/10.1038/s43246-021-00202-6>.

**Correspondence** and requests for materials should be addressed to Benjamin Winkeljann or Oliver Lieleg.

**Peer review information** *Communications Materials* thanks the anonymous reviewers for their contribution to the peer review of this work. Primary Handling Editor: John Plummer.

**Reprints and permission information** is available at <http://www.nature.com/reprints>

**Publisher's note** Springer Nature remains neutral with regard to jurisdictional claims in published maps and institutional affiliations.



**Open Access** This article is licensed under a Creative Commons Attribution 4.0 International License, which permits use, sharing, adaptation, distribution and reproduction in any medium or format, as long as you give appropriate credit to the original author(s) and the source, provide a link to the Creative Commons license, and indicate if changes were made. The images or other third party material in this article are included in the article's Creative Commons license, unless indicated otherwise in a credit line to the material. If material is not included in the article's Creative Commons license and your intended use is not permitted by statutory regulation or exceeds the permitted use, you will need to obtain permission directly from the copyright holder. To view a copy of this license, visit <http://creativecommons.org/licenses/by/4.0/>.

© The Author(s) 2021